

Article

Electric Vehicle Charging Demand Prediction Model Based on Spatiotemporal Attention Mechanism

Yang Chen ^{1,*}, Zeyang Tang ^{1,2}, Yibo Cui ², Wei Rao ² and Yiwen Li ²

¹ College of Electrical Engineering and New Energy, China Three Gorges University, Yichang 443002, China

² State Grid Hubei Electric Power Research Institute, Wuhan 430077, China

* Correspondence: 202208580121025@ctgu.edu.cn

Abstract: The accurate estimation and prediction of charging demand are crucial for the planning of charging infrastructure, grid layout, and the efficient operation of charging networks. To address the shortcomings of existing methods in utilizing the spatial interdependencies among urban regions, this paper proposes a forecasting approach that integrates dynamic time warping (DTW) with a spatial–temporal attention graph convolutional neural network (ASTGCN). First, this method delves into the correlations between various regions within the target city, establishing intricate coupling relationships among them. Subsequently, the FastDTW algorithm is employed to construct an adjacency matrix, capturing the spatiotemporal correlation among different urban regions. Finally, the ASTGCN model is applied to predict the power load of each region, which can accurately capture the spatiotemporal characteristics of the power load. The experimental results indicate that the proposed model has a more powerful comprehensive ability to capture spatiotemporal relationships and improve accuracy and stability in different prediction steps.

Keywords: electric vehicle; charging demand; spatiotemporal distribution; FastDTW; load forecasting



Academic Editor: Giovanni Lutzemberger

Received: 20 December 2024

Revised: 28 January 2025

Accepted: 30 January 2025

Published: 2 February 2025

Citation: Chen, Y.; Tang, Z.; Cui, Y.; Rao, W.; Li, Y. Electric Vehicle Charging Demand Prediction Model Based on Spatiotemporal Attention Mechanism. *Energies* **2025**, *18*, 687. <https://doi.org/10.3390/en18030687>

Copyright: © 2025 by the authors. Licensee MDPI, Basel, Switzerland. This article is an open access article distributed under the terms and conditions of the Creative Commons Attribution (CC BY) license (<https://creativecommons.org/licenses/by/4.0/>).

1. Introduction

Under the goal of achieving “carbon peaking and carbon neutrality”, electric vehicles (EVs) powered by renewable energy have emerged as critical enablers facilitating clean energy transitions in national power systems [1]. However, the uncoordinated integration of large-scale EVs results in high volatility and randomness in the load of the regional power grid [2], posing potential dangers to the grid [3]. Simultaneously, it introduces new challenges for electric load forecasting. Accurate prediction of EV charging station loads is not only fundamental to power grid load planning [4]; it also serves as a prerequisite for guiding EV charging and is of significant importance for promoting the planning of charging facilities [5]. At present, the current EV charging load prediction methodologies can be broadly categorized into statistical learning approaches and machine learning (ML)-based techniques [6]. Statistical learning methods primarily use statistical analysis techniques to model and analyze historical EV charging and discharging data to predict future charging loads [7]. In [8], the spatiotemporal distribution of charging loads is predicted based on the interaction information between the road network and the power grid, as well as user psychology. Yang, B et al. [9] established a large-scale EV charging demand model using Monte Carlo simulation by analyzing user driving patterns. Zhang, J. et al. [10] developed a probabilistic travel model for typical users based on statistical data on user charging preferences, charging power, and charging locations. Although these

conventional methods offer straightforward implementation, their predictive accuracy remains constrained by inherent limitations in data quality and sample size adequacy.

With the rapid development of artificial intelligence (AI) technology, machine learning (ML) methods are increasingly applied in charging load forecasting tasks [4]. In [11], a combination of convolutional neural networks and long short-term memory models is used to extract the spatial and temporal features of load data, enhancing the accuracy of short-term load forecasting. Wang, Y et al. [12] employed long short-term memory neural networks and support vector machines to predict subsequence charging demands, integrating the results through a stacking ensemble learning strategy. In [13], wavelet decomposition is utilized to extract the temporal and frequency domain information of renewable energy, combined with a bidirectional long short-term memory network model and an attention mechanism to mine deep data information. However, the methods mentioned above predominantly emphasize temporal dependencies while neglecting spatial heterogeneity in urban functional zones. In reality, the load demand characteristics across different functional areas in a city may differ significantly. For example, the peak load times and load volumes in commercial, residential, and industrial areas may vary considerably. In recent years, graph network algorithms have shown great potential in power system analysis due to their ability to capture complex network structures and dynamic interactions [14,15]. Therefore, Hu, B et al. [16] constructed a graph WaveNet charging load prediction framework using a learnable spatial adjacency matrix. Luo, R.K et al. [17] combined graph convolutional networks with gate recurrent units (GRUs) to predict the availability of charging stations. Zhuang et al. [18] introduced a sequential forecast-then-optimize framework for the real-time hosting capacity assessment of electric vehicles, dynamically updating grid models to enhance responsiveness to charging demand. Mekkaoui et al. [19] proposed a probabilistic dual-adaptive spatiotemporal GCN, which dynamically adjusts spatiotemporal weights between nodes to effectively capture the dynamic energy consumption patterns of charging stations, offering novel insights for modeling dynamically changing spatial relationships. Although some studies have begun to explore the application of graph networks in charging load prediction, existing research on this field remains insufficient. In particular, studies that combine spatial-temporal attention mechanisms with graph networks are relatively rare, yet this combination is one of the key factors in improving prediction accuracy.

These models account for the complex spatiotemporal dependencies of charging loads between different charging stations. However, they still face the following issues: (1) The adjacency matrix in graph networks typically uses actual geographical location information between nodes. However, the influence of geographic factors is often not directly reflected on the surface and requires deeper exploration of the latent relationships between nodes. (2) The models typically only input charging load data, lacking feature dimension inputs. The electric vehicle charging load in a particular area is highly related to the current traffic flow, which is dynamically influenced by the traffic conditions of different regions. Capturing these dynamically changing spatial relationships in a model remains challenging in current research.

In practice, while individual EV charging behavior exhibits strong randomness and unpredictability, cluster-level analysis reveals discernible similarities in charging load characteristics across vehicles within the same regional category. Based on this, this paper proposes an innovative forecasting approach. First, through in-depth cross-correlation analysis, the complex correlations between charging loads in different regions are precisely quantified, revealing the underlying coupling information. Second, the FastDTW algorithm is used to construct the adjacency matrix, capturing and reinforcing intrinsic cross-regional charging load dependencies. This adjacency matrix is then input into a combined model

of spatial-temporal attention mechanisms and graph convolutional networks, enabling the model to more flexibly and accurately capture the spatiotemporal evolution patterns of charging loads. Additionally, by introducing spatial attention, the model allows for the “dynamic” adjustment of the graph topology structure through varying spatial attention weights, thus addressing the dynamic changes in traffic flow and ultimately achieving accurate charging demand prediction.

2. Materials and Method

2.1. Spatial Cross-Correlation Analysis

In previous research, load cells (hereinafter referred to as cells) are often divided based on either equally sized grids or into irregular (Type I cells) or regular (Type II cells) cells [20]. For qualitative analysis and experimental validation, this paper uses an area in Wuhan as an example, adopting the division rules of Type I cells. User-level cells are constructed in alignment with the spatial framework defined in the “Wuhan Main Functional Area Plan” [21]. Dividing cells according to different functional areas facilitates spatial load forecasting by leveraging spatial relationships for research and exploration.

It should be noted that the user-level cells mainly depend on land use attributes, such as commercial, industrial, and residential properties. These land use attributes determine the variation patterns of electric vehicle charging loads, and since the cells are located close to each other, they experience consistent weather conditions. Therefore, it can be assumed that meteorological factors do not affect the charging load in the current study area.

To validate the correlation between charging loads in different regions, this paper analyzes the correlation from three perspectives: Pearson correlation coefficient, Spearman correlation coefficient, and Kendall correlation coefficient. The Pearson correlation coefficient [22], which measures linear relationships between two variables x and y , is expressed by the following formula:

$$R_{xy} = \frac{\sum_{i=1}^n (x_i - \bar{x})(y_i - \bar{y})}{\sqrt{\sum_{i=1}^n (x_i - \bar{x})^2} \sqrt{\sum_{i=1}^n (y_i - \bar{y})^2}} \quad (1)$$

where x_i and y_i are the values of the variables x and y at the i -th data point; \bar{x} and \bar{y} are the means of x and y ; and n denotes the number of data points or variable values.

The Spearman correlation coefficient [23] quantifies the monotonic relationship between two variables by analyzing the ranks of the values rather than the values themselves. It measures the strength and direction of the monotonic relationship. For a sample size of n , the formula for calculating the Spearman correlation coefficient is as follows:

$$\rho = 1 - \frac{6\sum d_i^2}{n(n^2 - 1)} \quad (2)$$

where d_i represents the rank difference between the i -th values of x_i and y_i , and n is the number of data points or variable values.

The Kendall correlation coefficient [24] is another rank-based correlation coefficient used to assess the general correlation between variables. It reflects both monotonic and non-monotonic relationships. The Kendall correlation coefficient is denoted by τ , and its formula is as follows:

$$\tau = \frac{C - D}{\sqrt{(C + D + T)(C + D + U)}} \quad (3)$$

where C is the number of concordant pairs (pairs of observations where the ranks for both variables agree in order); D is the number of discordant pairs (pairs of observations where the ranks for both variables disagree in order); and T and U are the number of tied ranks for x and y , respectively.

The three correlation coefficients provide insights into the relationships between regions from linear, monotonic, and general correlation perspectives, respectively. The results of the calculations are shown in Figure 1. From the three correlation graphs, it is clear that the relationships between the prediction target and influencing factors remain consistent despite using different correlation coefficients for evaluation. There are notable differences in the correlations between different functional areas, revealing potential coupling information between them. If the charging load in one region suddenly increases, it can be predicted that the charging load in other regions may also increase. This information is crucial for grid planning and operation as it helps power companies better manage electricity demand and allocate resources. Traditional models face difficulties in extracting spatial features due to their inability to share information. Therefore, constructing a graph matrix using information from different regions and weaving the charging load data from each region into a network enhances the model's ability to extract features.

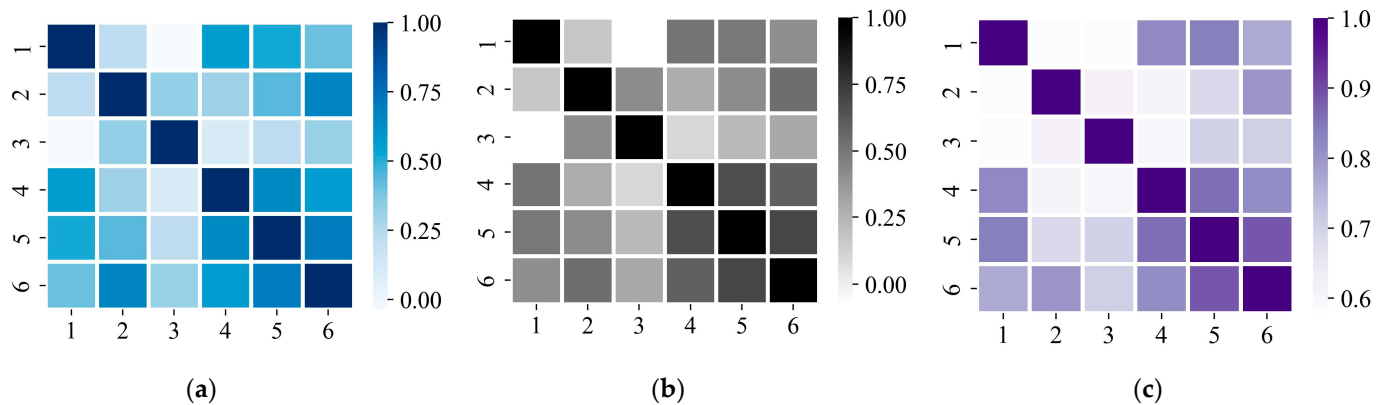


Figure 1. Heatmaps of regional correlation coefficients: (a) Pearson correlation coefficient matrix; (b) Spearman correlation coefficient matrix; (c) Kendall correlation coefficient matrix.

2.2. Fast Dynamic Time Warping (FastDTW) Algorithm

Travel patterns influence the charging load of electric vehicles, and the charging load time series between different regions may exhibit non-linearity and asynchrony, meaning that their load variation patterns may occur at different time points but still share similarities. FastDTW is an enhanced variant of the dynamic time warping (DTW) algorithm, designed to compute the optimal alignment path between two time series with reduced computational complexity. This enables the algorithm to capture the similarity between the sequences effectively. Unlike the traditional DTW algorithm, FastDTW employs a multi-level approach that significantly lowers the computational burden, thereby facilitating the more efficient processing of large-scale datasets. Traditional graph networks typically use the actual geographical distance between nodes to construct the adjacency matrix. However, in reality, geographical factors do not always have an obvious impact, and deeper latent relationships between nodes need to be explored. In this paper, we replace geographic location with the FastDTW algorithm. Let the charging load time series of the n -th region at period t be denoted as $x_n = (x_{n,1}, x_{n,2}, \dots, x_{n,t})$. The distance matrix D between x_n and x_{n-1} is computed using the FastDTW algorithm. The specific formula is as follows:

$$d(i, j) = F_DTW(i, j) \quad (4)$$

$$D = \begin{bmatrix} d(1,1) & d(1,2) & \cdots & d(1,n) \\ d(2,1) & d(2,2) & \cdots & d(2,n) \\ \vdots & \vdots & \ddots & \vdots \\ d(n,1) & d(n,2) & \cdots & d(n,n) \end{bmatrix} \quad (5)$$

The distance matrix D is a symmetric $N \times N$ matrix, where N denotes the number of regions. Each entry $D_{i,j}$ quantifies the temporal alignment distance between regions i and j , ensuring bidirectional correlation modeling. To incorporate both temporal and spatial information into the adjacency matrix that reflects the interactions between regions, this paper uses the distance matrix D obtained from the FastDTW algorithm, along with the Sigmoid function, to construct the adjacency matrix A . The elements of the adjacency matrix A can be expressed as follows:

$$A_{ij} = \begin{cases} \sigma(d(i,j)) & i \neq j \\ 1 & i = j \end{cases} \quad (6)$$

where σ is the Sigmoid function.

2.3. Time Series Feature Analysis

Figure 2 shows the variation in charging demand intensity for Region 2 over a week. Observations indicate that the daily charging demand exhibits a certain degree of similarity and regularity. Early in the day, charging demand is relatively low. As time progresses, the demand increases, reaching a peak, and then decreases during the evening until early the next day. The charging demand data shows distinct peaks and valleys corresponding to time changes, which is a typical pattern influenced by people's daily routines. Due to the strong similarity in charging demand at the same time each day, the prediction model for charging demand in this paper should account for the daily periodicity present in the charging demand data.

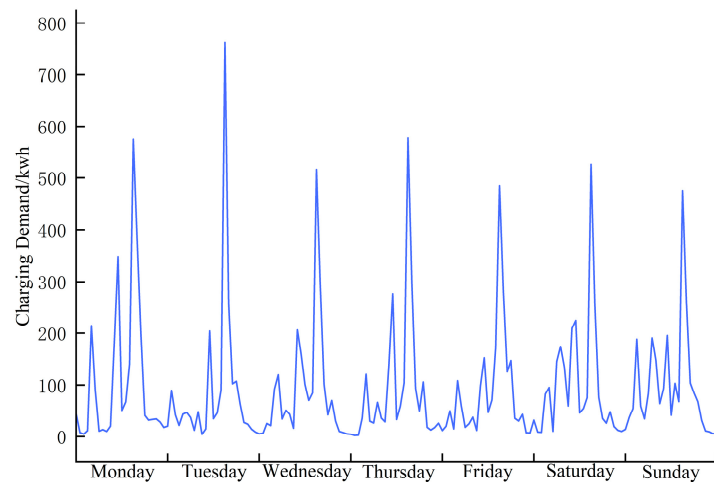


Figure 2. Daily charging demand diagram.

Figure 3 illustrates the changes in charging demand intensity for the first and second weeks of March 2021. Observations reveal that the charging demand data for these two weeks are similar, with the trends in charging demand on the same weekdays and weekends also showing high similarity. The temporal distribution of charging demand maintains a certain level of stability, and the data exhibit distinct and similar peaks and valleys over time. Therefore, the charging demand prediction model in this paper should consider the weekly periodicity present in the electric vehicle charging demand.

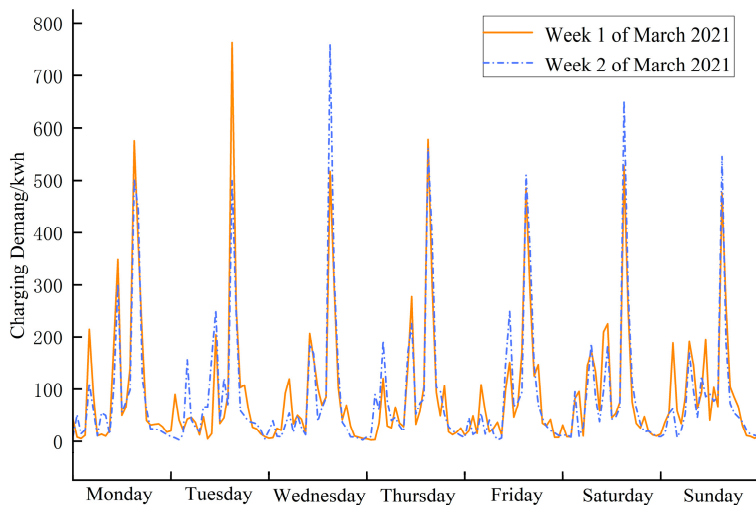


Figure 3. Weekly charging demand diagram.

2.4. Charging Load Prediction Framework

In this paper, we represent the graph structure of each region using $G = (V, E, A)$, where V is the set of charging region nodes, E is the set of edges between the charging regions, and A is the adjacency matrix. As shown in Figure 4, the weight of an edge represents the correlation strength between the loads of two charging regions. The spatiotemporal graph data format is defined as follows: (adjacency matrix; number of nodes, number of features, time steps). In this context, each region cell corresponds to a node in the graph, and the adjacency matrix corresponds to the edge relationships in the graph. The load feature is a time-varying parameter matrix, X_t , which includes the feature values of each node sampled at the same frequency. Let $X_t = [x_t^1, x_t^2, \dots, x_t^N]$ represent the historical feature values of N charging load nodes at time t , where $x_t^i = [x_t^{1,i}, x_t^{2,i}, \dots, x_t^{F,i}]$ denotes the F feature values of the i -th charging load node at time t . Therefore, the charging load dataset of N charging load nodes over T time steps can be represented as a three-dimensional array $X = [X_1, X_2, \dots, X_T] \in \mathbb{R}^{N \times F \times T}$. According to the above definitions, given the historical data values X of all nodes in the charging regions over the past τ time steps, we aim to predict the future load value sequence $Y = (y^1, y^2, \dots, y^N) \in \mathbb{R}^{N \times T_p}$ of all nodes in the charging regions for the next T_p time steps. Here, $y^i = (y_{\tau+1}^i, y_{\tau+2}^i, \dots, y_{\tau+T_p}^i) \in \mathbb{R}^{T_p}$ represents the future load value of node i starting from time τ .

This paper introduces an attention-based spatiotemporal graph convolutional network (ASTGCN) model as the foundation for electric vehicle charging load prediction, as shown in Figure 5. The model consists of three structurally identical periodic dependency components, each designed to capture the temporal characteristics in the recent, daily-periodic, and weekly-periodic segments. Specifically, the inputs for the recent segment, the daily-periodic segment, and the weekly-periodic segment are time series segments of length T_h , T_d , and T_w , respectively. The core of each component is the spatial-temporal blocks (STblock), which comprises a spatiotemporal feature extraction layer (SAttn + TAttn) and a spatiotemporal convolutional layer (CNN + GCN). The spatiotemporal feature extraction layer consists of the spatial attention mechanism (SAttn) and the temporal attention mechanism (TAttn), and its primary role is to capture the dynamic spatiotemporal correlations across the charging regions. The spatiotemporal convolutional layer includes spatial graph convolution (GCN) and temporal convolution (CNN), which serve to mine the spatiotemporal features of the load data. The model first uses the FastDTW algorithm to analyze the charging load time series across different regions, identifying the optimal matching paths. These cumulative distances are then transformed into an adjacency matrix,

providing spatial relationship information for the graph convolution network. The graph convolution layer uses this adjacency matrix to model the topology of the charging areas, while the temporal and spatial attention modules, respectively, apply weighting to the features of the time series and spatial distribution to emphasize the most critical time points and regions for prediction. As a result, the spatiotemporal modules are highly effective in capturing the dynamic spatiotemporal patterns of the load data. Stacking multiple spatiotemporal modules allows for a richer extraction of dynamic spatiotemporal patterns. The connections between spatiotemporal modules are achieved through residual links, which improve the training efficiency and stability of the model. Finally, the prediction results are weighted across three time scales, namely, recent, daily-periodic, and weekly-periodic, and the features from these three different periodic components are integrated. To ensure that the output dimensions of the model align with the prediction target dimensions, a fully connected network is used to map the component output dimensions to the target dimensions, producing the final prediction results. This approach enables the precise forecasting of future charging loads for each region.

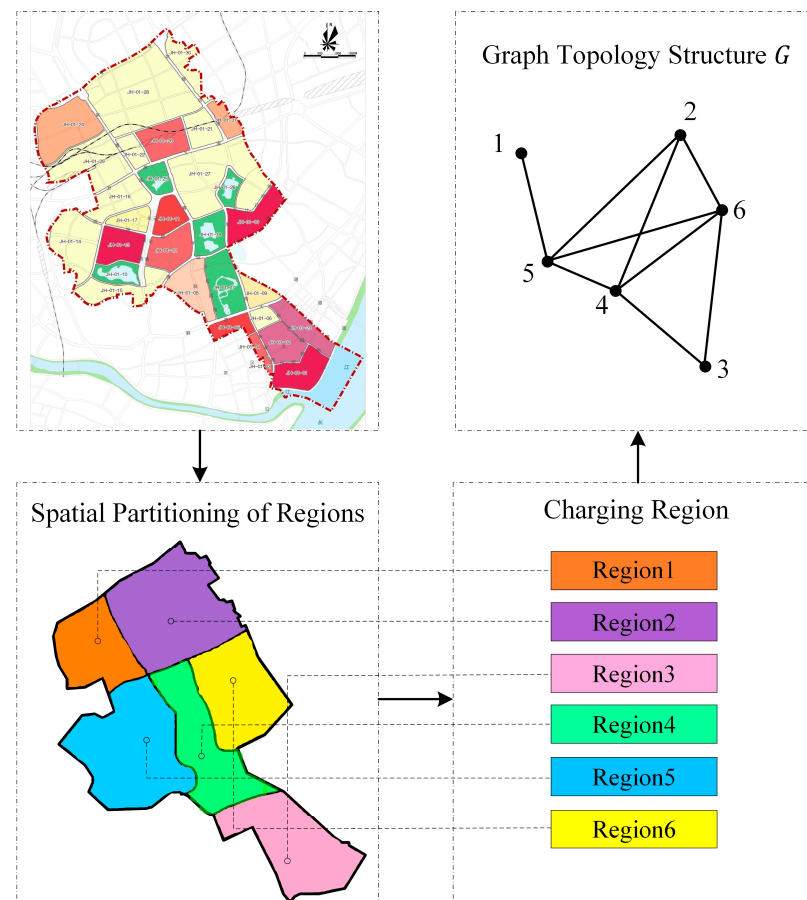


Figure 4. Diagram of regional graph topology construction.

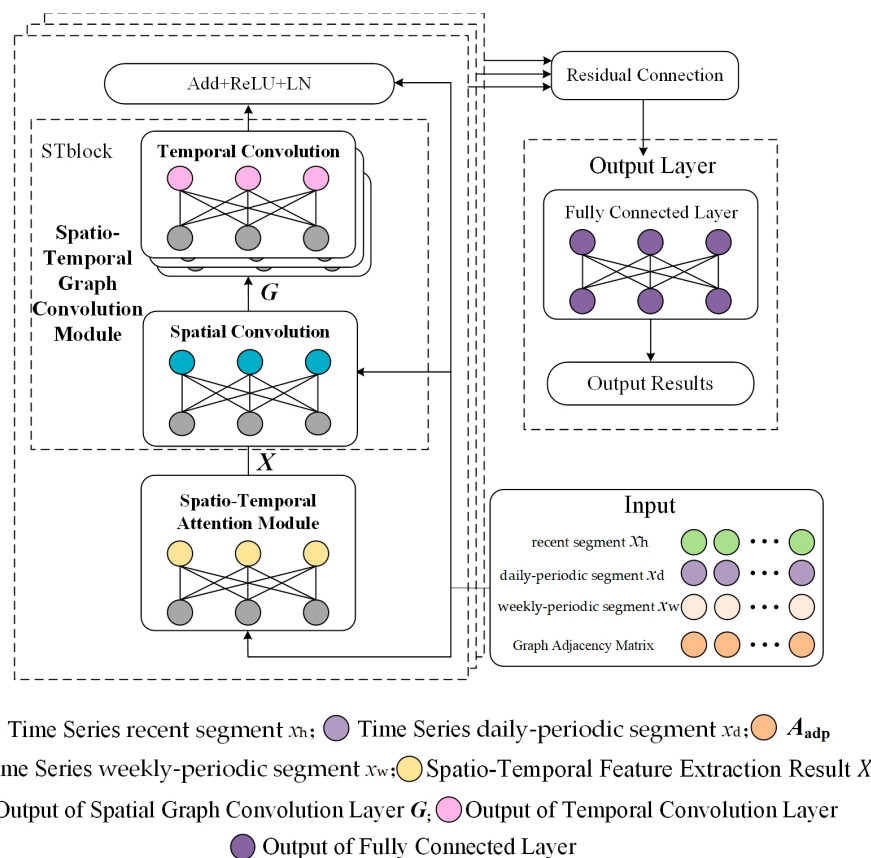


Figure 5. Model framework.

2.5. Spatiotemporal Attention Mechanism

Electric vehicle charging load prediction is a complex task because it is influenced not only by temporal data but also by spatial distribution data. Graph networks are capable of handling graph topology and the interactions between nodes, while the spatiotemporal attention mechanism can capture important features in both time and space [25], as well as the dependencies between them. The attention mechanism dynamically adjusts the weights based on historical and real-time data, emphasizing the time points and spatial regions most critical for the current prediction. The spatiotemporal attention mechanism adaptively captures the dynamic correlations between nodes in the time and space dimensions by calculating a spatiotemporal attention matrix, as shown in Figure 6. The calculation formula is as follows:

$$SAM'_{i,j} = \text{softmax}(V_s \cdot \sigma((X_h^{(k-1)} W_1) W_2 (W_3 X_h^{(k-1)})^T + b_s)) \quad (7)$$

$$TAM'_{i,j} = \text{softmax}(V_t \cdot \sigma(((X_h^{(k-1)})^T U_1) U_2 (U_3 X_h^{(k-1)})^T + b_t)) \quad (8)$$

where $X_h^{(k-1)} = (X_1, X_2, \dots, X_{T_{k-1}}) \in \mathbb{R}^{N \times F_{k-1} \times T_{k-1}}$ is the input to the k -th spatial-temporal block, and F_{k-1} is the number of input data channels in the k -th layer. T_{k-1} represents the length of the temporal dimension in the k -th layer. $V_s, b_s, V_t, b_t \in \mathbb{R}^{N \times N}$, $W_1, U_1 \in \mathbb{R}^{T_{k-1}}$, $W_2, U_2 \in \mathbb{R}^{F_{k-1} \times T_{k-1}}$, and $W_3, U_3 \in \mathbb{R}^{F_{k-1}}$ are learnable parameters. The sigmoid function σ is used as the activation function to compute the attention scores for each graph. Then, the SoftMax function is applied to normalize the weights, ensuring that the sum of the weight coefficients equals 1. This process results in the standardized spatial attention score matrix $SAM'_{i,j}$ and the temporal attention score matrix $TAM'_{i,j}$.

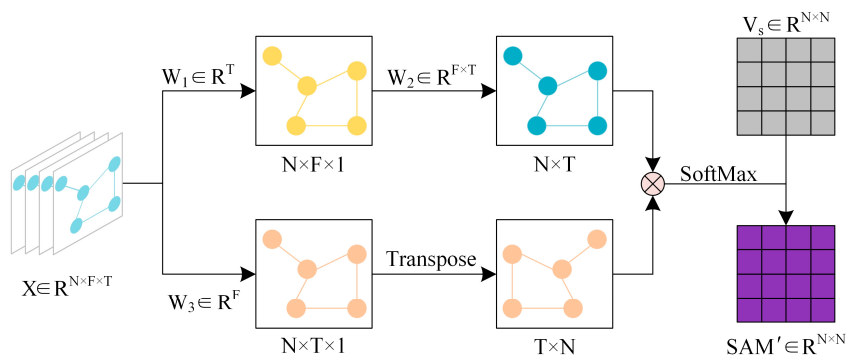


Figure 6. Spatial attention mechanism calculation process.

2.6. Graph Convolutional Networks

The urban power grid is essentially a complex graph structure, where each city area can be viewed as a node in the graph. The interactions and dependencies between these regions form a complex network structure, and graph networks [26] serve as an effective tool for handling such complex network structures, enabling the transmission of information and feature extraction through the connections between nodes. This paper is based on graph convolutional networks (GCN) and utilizes Chebyshev polynomial approximations to learn topological features, applying graph convolution directly on each time slice to process the input, as shown in Equation (9):

$$g_\theta *_G x \approx g_\theta(\mathbf{L})x = \sum_{k=0}^{K-1} \theta_k T_k(\tilde{\mathbf{L}})x \quad (9)$$

where $*$ denotes the standard convolution operation; θ_k is the coefficient of the k -th term of the Chebyshev polynomial; K is the total number of polynomial terms; $T_k(\cdot)$ is the Chebyshev polynomial introduced for recursive computation; $T_k(X) = 2XT_{k-1}(X) - T_{k-2}(X)$; and $\tilde{\mathbf{L}} = \frac{2}{\lambda_{max}}\mathbf{L} - I_N$, where λ_{max} is the largest eigenvalue of L .

In the spatial dimension, each term $T_k(\tilde{\mathbf{L}})$ in Equation (9) is operated with $SAM'_{i,j}$, obtained from Equation (7), resulting in $T_k(\tilde{\mathbf{L}}) \odot SAM'$, where \odot denotes the Hadamard product. Finally, the graph convolution operation based on the spatial attention mechanism can be expressed as follows:

$$g_\theta *_G x = g_\theta(\mathbf{L})x = \sum_{k=0}^{K-1} \theta_k (T_k(\tilde{\mathbf{L}}) \odot SAM')x \quad (10)$$

In the temporal dimension, after modeling the spatial dimension using GCN, the temporal dimension of the data is modeled based on standard 2D convolution. This standard convolution operation in the temporal dimension updates the information of a node using the information from adjacent time steps, employing *ReLU* as the activation function. The result of the temporal convolution operation is shown in Equation (9), yielding the output of the h -th layer X_h^k :

$$X_h^k = \text{ReLU}(\Phi * (\text{ReLU}(g_\theta *_G \hat{X}_h^{(k-1)}))) \quad (11)$$

where $*$ denotes the standard convolution operation, and Φ represents the parameters of the convolution kernel in the temporal dimension. In electric vehicle load prediction, the combination of graph convolution and spatiotemporal attention can simultaneously capture the topological structure of urban electric vehicle charging nodes, the interactions between charging areas, and important temporal and spatial features, thereby improving

the prediction accuracy. Graph convolution handles the graph structure of charging nodes, capturing the dependencies between different charging regions, while spatiotemporal attention dynamically emphasizes the most influential time points and spatial nodes for the prediction results. The integration of these two components allows the model to gain a more comprehensive and in-depth understanding of the variation patterns in charging loads.

3. Results

3.1. Data Process

This study utilizes real-world electric vehicle (EV) operational data collected from sensor networks in Wuhan, China, spanning 1 January to 31 March 2021. As shown in Table 1, the raw dataset comprises seven fields: vehicle ID, timestamp (UTC milliseconds), longitude and latitude (raw geographic coordinates), charging status (binary: 0 for idle; 1 for charging), voltage (V), and current (A). Based on Wuhan's Main Functional Area Plan, longitude and latitude coordinates were mapped to six predefined functional regions (cells), including commercial, residential, and industrial zones. Charging loads for each region were aggregated hourly by calculating the total energy consumption (kWh) using voltage and current measurements:

$$P = \sum(V_i \times I_i \times \Delta t)/1000 \quad (12)$$

where V_i and I_i represent the voltage and current of the i -th vehicle, and $\Delta t = 1$ h. The pre-processing pipeline began with data cleaning to ensure temporal continuity and reliability. Records with zero power values during charging events were identified as invalid and replaced using linear interpolation. Abrupt load fluctuations caused by sensor noise, defined as deviations exceeding ± 3 standard deviations from the hourly mean, were smoothed via local averaging. Subsequent feature engineering focused on encoding temporal patterns and normalizing numerical features. Temporal attributes (year, month, day, hour, weekday) were one-hot encoded to capture periodic trends, while traffic flow (number of EVs per region) and historical load (kWh) were normalized to the range [0, 1] via min–max scaling to mitigate feature scale discrepancies:

$$\hat{X}_t = \frac{X_t - X_{\min}}{X_{\max} - X_{\min}} \quad (13)$$

Table 1. Original dataset labels.

Vehicle ID	Time	Charging Status	Longitude	Latitude	Voltage	Current
1468xxxxe8	1.61×10^{12}	1	114.xxxx	30.xxxx	397.x	60.x
1468xxxxe8	1.61×10^{12}	1	114.xxxx	30.xxxx	398.x	62.x
1468xxxxe8	1.61×10^{12}	1	114.xxxx	30.xxxx	398.x	74.x
...

The preprocessed data were structured into a spatiotemporal tensor $X \in R^{6 \times 3 \times 168}$, where dimensions correspond to 6 regions, 3 features (traffic flow, load, encoded time), and 168 historical hourly steps (Table 2). To evaluate model performance, the dataset was partitioned into training (1 January–10 March, 80%) and testing (11–31 March, 20%) sets, preserving temporal coherence and avoiding data leakage.

Table 2. Model input dataset.

Input Type	Specific Name	Symbol	Unit	Meaning
Time Information	Year	Y		
	Month	M		
	Day	D	N/A	Time label
	Hour	H		
	Weekday	W	N/A	Whether it is a weekday
Traffic Flow	Traffic Flow	S	veh/h	Number of electric vehicles
Load Information	Historical Load	P	KWh	Electric vehicle charging load

Entries marked with N/A in the 'Unit' column denote parameters that are one-hot encoding and thus unitless.

3.2. Model Parameter Settings and Evaluation Metrics

3.2.1. Hyperparameter Settings

Current research suggests that the combination model of CNN and LSTM, known as CNN-LSTM, performs well. The spatiotemporal graph convolutional network (STGCN) is a classic model for spatiotemporal data. Therefore, LSTM, GRU, CNN-LSTM-ATTENTION, and STGCN are used as comparison models in this study. LSTM, GRU, and CNN-LSTM do not consider spatial relationships, whereas STGCN introduces GCN to account for spatial relationships based on CNN-GRU.

The specific parameters of the ASTGCN model are as follows: the number of layers in the spatiotemporal module is 2, the batch size is 32, the number of iterations is 100, the learning rate is 0.001. The training algorithm used is Adam. Additionally, in this study, N is set to 6, T_p to 24, and F to 3.

3.2.2. Evaluation Metrics

This paper selects the root mean squared error (I_{RMSE}), mean absolute error (I_{MAE}), and mean absolute percentage error (I_{MAPE}) as the metrics for evaluating the predictive performance of various models. The calculation formulae are as follows:

$$I_{RMSE} = \sqrt{\frac{1}{NT} \sum_{t=1}^T \sum_{i=1}^N (f_{i,t} - F_{i,t})^2} \quad (14)$$

$$I_{MAE} = \frac{1}{NT} \sum_{t=1}^T \sum_{i=1}^N |f_{i,t} - F_{i,t}| \quad (15)$$

$$I_{MAPE} = \frac{1}{NT} \sum_{t=1}^T \sum_{i=1}^N \left| \frac{f_{i,t} - F_{i,t}}{f_{i,t}} \right| \quad (16)$$

where $f_{i,t}$ and $F_{i,t}$ represent the actual value and the predicted value at time t for the i -th cell, respectively.

3.3. Results Analysis

This study implements the ASTGCN model and baseline comparison models using the PyTorch 1.8.0 deep learning framework, with experiments conducted on a system equipped with an AMD Ryzen 7 7840H processor (Advanced Micro Devices, Inc., Santa Clara, CA, USA) and an NVIDIA GeForce RTX 4060 8 GB GPU (NVIDIA Corporation, Santa Clara, CA, USA). Using a multi-output, multi-step prediction strategy. These models predict the charging load for six charging regions, using the historical data of the past 168 h to forecast the load for the next 24 h (Figure 7). The I_{MAE} and I_{RMSE} metrics comparison for the five models is shown in Figure 8. It can be observed that the spatiotemporal graph convolutional

network (STGCN) slightly outperforms the GRU and LSTM networks. This is because the STGCN can effectively extract spatiotemporal features by combining TGCN and GCN, resulting in higher prediction accuracy than traditional time series prediction models.

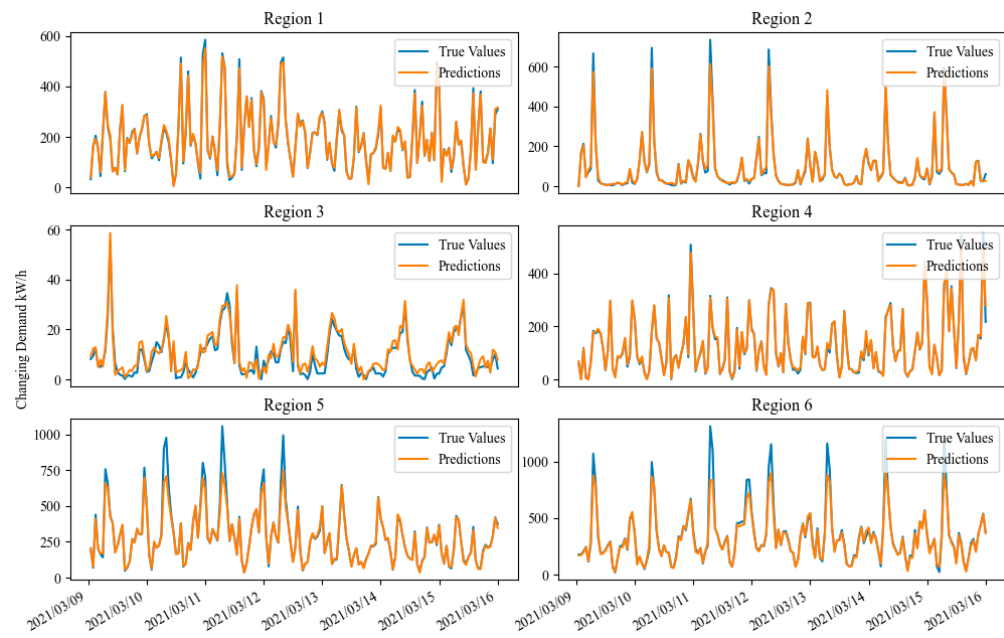


Figure 7. Forecasting curve comparison graph of the FastDTW-ASTGCN model.

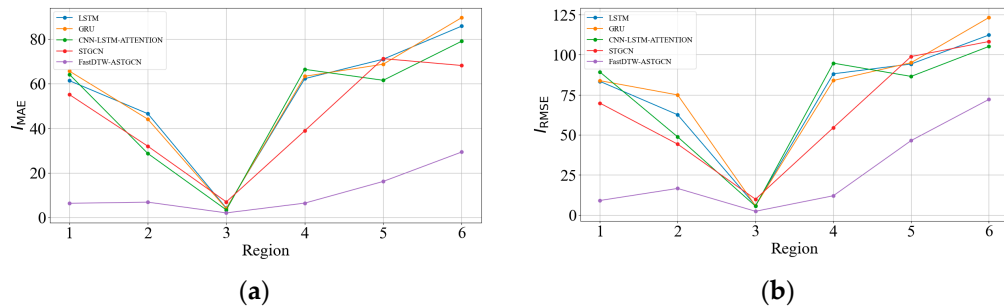


Figure 8. Performance measures of proposed models: (a) MAE; (b) RMSE.

The GCN model is compared with the CNN model to verify the prediction accuracy of the graph topology construction method proposed in this paper. Additionally, to validate the effectiveness of the spatiotemporal attention mechanism in enhancing model prediction performance, the ASTGCN model is compared with the STGCN model.

In the prediction of electric vehicle charging load, taking region 2 as an example, the following conclusions were drawn: among the five models, the ASTGCN model achieved the best prediction performance, with the lowest I_{MAE} . Compared to the CNN-LSTM-ATTENTION model, the proposed model improved RMSE and MAE by 45.96% and 52.01%, respectively, indicating that the proposed graph topology construction method better represents the spatial relationships among the charging regions. Compared to the STGCN model, RMSE and MAE were improved by 32.48% and 38.46%, respectively, demonstrating that the introduction of the spatiotemporal attention mechanism in the proposed model effectively captures spatiotemporal features. Compared to the GRU model, RMSE decreased by up to 51.33 kWh, and MAE decreased by up to 44.67 kWh; compared to the LSTM model, RMSE decreased by up to 48.96 kWh, and MAE decreased by up to 43.96 kWh.

4. Discussion

4.1. DTW Performance Evaluation

The parameter settings of the adjacency matrix A are crucial for graph-based models, as A determines which historical load and feature data from neighboring cells are incorporated. In this case, the predictive results are compared by constructing the adjacency matrix using different correlation metrics, including Pearson correlation coefficient, Spearman correlation coefficient, Kendall rank correlation coefficient, and dynamic time warping distance. The specific matrix parameters can be found in Appendix A. The results of different adjacency matrix settings are shown in Table 3.

Table 3. Result of different adjacency matrices.

Adjacency Matrix	STGCN			ASTGCN		
	I _{RMSE}	I _{MAE}	I _{MAPE} /%	I _{RMSE}	I _{MAE}	I _{MAPE} /%
A1	60.21	42.76	0.78	35.84	16.44	0.46
A2	64.22	45.39	0.83	38.67	17.70	0.49
A3	58.56	39.42	0.74	34.73	14.85	0.43
A4	56.47	37.81	0.71	32.44	13.51	0.37
A*	55.39	36.46	0.69	28.81	11.22	0.34

Compared to the Pearson correlation coefficient (corresponding to adjacency matrix A1), Spearman correlation coefficient (corresponding to adjacency matrix A2), and Kendall rank correlation coefficient (corresponding to adjacency matrix A3), the dynamic time warping algorithm (corresponding to adjacency matrix A4) consistently achieves the smallest error in the comparative experiments of STGCN and ASTGCN models. FastDTW demonstrates a clear advantage in handling electric vehicle charging load time series data.

During the experiment, it was found that regional information from the same direction could lead to data redundancy as too many repetitive or similar samples might cause uneven data distribution. Adjustments were made to A1–A4, specifically modifying some cells in A4 by removing the correlations between cells 1 and 4, cells 2 and 5, cells 3 and 4, cell 4 and cell 6, and cell 5 and cell 6. Under the adjacency matrix parameter A*, both the STGCN and ASTGCN models showed significant performance improvement. This demonstrates that the parameter settings of the adjacency matrix are crucial for the prediction performance of the graph model. Although A* and other adjacency matrices only differ in some adjacency relationships, the final prediction results differ significantly. Therefore, when selecting the adjacency matrix, it is essential to consider regional information from multiple neighboring directions to avoid the data redundancy caused by regions in the same direction and to choose an appropriate graph model adjacency matrix.

4.2. ASTGCN Performance Evaluation

To investigate the impact of time step length on demand forecasting, charging demand data were converted into time series using time steps of 1 h, 24 h, 72 h, and 168 h, respectively. The prediction performance of the ASTGCN model and various benchmark models at different time step lengths is shown in Table 4. As can be seen from the table, the ASTGCN model achieved the best prediction results across all charging demand time series with different time step lengths, demonstrating its relative stability and accuracy in predicting charging demand data. Moreover, compared to other benchmark models, the performance degradation of the attention-based spatial-temporal graph convolutional network model was slower as the time step length increased, highlighting its relative stability in prediction performance and its applicability to both short-term and long-term

charging demand forecasting. These results indicate that the ASTGCN model can enhance prediction performance by effectively extracting the spatial–temporal correlations in the charging demand data.

Table 4. Forecasting evaluation results for different prediction step lengths.

Prediction Time Step T_p/h	LSTM			GRU			CNN-LSTM			STGCN			ASTGCN		
	MAE	RMSE	T_e/s	MAE	RMSE	T_e/s	MAE	RMSE	T_e/s	MAE	RMSE	T_e/s	MAE	RMSE	T_e/s
1	55.18	74.38	18	55.89	77.75	17	50.53	71.62	32	45.39	64.22	46	11.22	28.81	64
24	54.62	72.13	18	54.91	76.29	17	49.62	69.87	32	44.67	66.31	46	11.43	29.75	64
72	58.73	78.93	18	57.27	78.33	17	52.39	73.66	32	46.22	67.59	46	11.79	36.46	64
168	61.84	80.63	18	66.35	79.84	17	55.72	75.92	32	48.96	69.35	46	13.68	39.59	64

In analyzing the computational complexity of the models, architectures based on recurrent neural networks (e.g., LSTM and GRU) exhibit lower computational overhead due to their straightforward modeling of temporal dependencies, with complexity primarily governed by sequence length and hidden layer dimensions. In contrast, CNN-LSTM models augmented with attention mechanisms introduce additional computations for local feature extraction and temporal focus, though their complexity remains manageable through linear combinations of convolutional kernels and attention weights. Graph convolutional networks (e.g., STGCN), which aggregate structural information across nodes, face significantly higher computational demands due to the need to process graph edges and node interactions. The proposed ASTGCN model extends STGCN by integrating spatiotemporal attention mechanisms, dynamically adjusting spatial and temporal weights to capture intricate dependencies. While this introduces a computational burden proportional to the square of the number of nodes, it substantially enhances the model's ability to prioritize critical regions and time intervals, leading to superior prediction accuracy. Although the spatiotemporal attention mechanism poses challenges for real-time deployment, strategies such as precomputing static adjacency matrices or sparsifying attention weights can optimize computational efficiency without sacrificing performance.

In addition, this study uses the components of neighboring dependency, daily periodicity, and weekly periodicity as inputs. The input data segment lengths, denoted as T_h , T_d , and T_w , are integer multiples of the predicted charging demand time T_p . Three groups of experiments were designed to explore the impact of these segment lengths on prediction results, with ASTGCN as the model. In these experiments, T_h , T_d , and T_w were set to one, two, and three times T_p , respectively. Different time steps were selected, and the experimental results are shown in Table 5. The results indicate that when T_h , T_d , and T_w are set to one times T_p , the model receives insufficient input data, leading to an inability to effectively capture the characteristic information of the charging demand, resulting in lower prediction accuracy. Conversely, when T_h , T_d , and T_w are set to three times T_p , the additional information overhead introduced by the increased input data reduces the model's prediction accuracy. The optimal prediction performance is achieved when T_h , T_d , and T_w are set to two times T_p .

To rigorously validate the effectiveness of each component in the ASTGCN model, we conducted an ablation study, as summarized in Table 6. The experimental results demonstrate that removing any critical module leads to significant performance degradation, thereby confirming the rationality of our model design. Replacing the FastDTW algorithm with geographic distance elevates MAE and RMSE by 33.46% and 36.16%, respectively, which underscores FastDTW's superiority in uncovering non-linear spatiotemporal correlation. Removal of the spatiotemporal attention mechanism increases MAE and RMSE by 47.76% and 56.78%, respectively, highlighting its essential role in dynamically assigning spatiotemporal weights to capture interdependencies across regions.

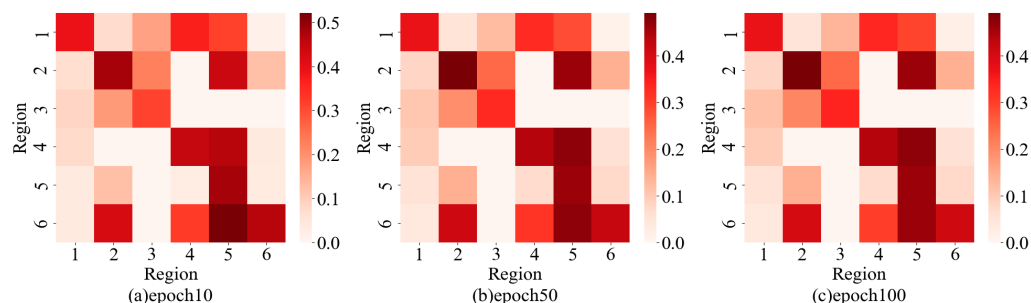
Table 5. Comparison of forecasting results for different input data lengths.

Evaluation Metrics	Group	1 h	24 h	72 h
MAE	1	8.68	11.62	12
	2	8.26	11.43	11.79
	3	8.57	11.56	11.86
RMSE	1	26.85	30.02	39.74
	2	25.96	29.75	39.46
	3	26.27	29.88	39.67

Table 6. Ablation study of the ASTGCN model components.

Model Variant	MAE (kWh)	RMSE (kWh)	MAPE (%)
Full ASTGCN	11.22	28.81	0.34
ASTGCN w/o FastDTW	17.34	39.23	0.47
ASTGCN w/o S-T Attention	21.48	45.17	0.62

The visualization of attention weight parameters is an advantage of the ASTGCN model presented in this paper. Compared to the STGCN model, which is also a graph model, the proposed model allows for a more intuitive analysis of the spatial dependencies between different charging regions. Figure 9 shows the attention weight heatmap of the ASTGCN model. As shown in Figure 5, the correlation degree between different regions is evident. For example, the load of region 6 is closely related to the loads of regions 2, 4, and 5. This is reasonable because regions 2, 5, and 6 are all residential areas, leading to higher attention weights for regions 2 and 5. Region 4 is adjacent to region 6, so its attention weight is slightly lower by comparison. By analyzing these spatial dependencies, utilities can prioritize charging infrastructure deployment in transitional zones between residential and commercial areas (e.g., near regions 2,6), where commuter-driven demand peaks occur daily. Meanwhile, the moderate link between region 6 and the adjacent region 4 (commercial area) highlights secondary-demand hotspots. By transforming abstract spatial dependencies into interpretable visual tools, the ASTGCN model bridges the gap between predictive analytics and operational decision-making, empowering utilities to align EV infrastructure investments and grid management strategies with observed behavioral and spatial trends.

**Figure 9.** Heatmap of attention weights.

5. Conclusions

This paper extends the definition of cells in the spatial scale for electric vehicle charging load prediction and proposes an electric vehicle charging load prediction model based on FastDTW-ASTGCN. The model integrates the unique advantages of both the FastDTW algorithm and the ASTGCN model, enabling accurate capture of the complex spatiotemporal features of urban electric vehicle charging loads, as well as the coupling relationships between different regions. The advantages of this model are as follows:

- (1) The proposed model achieves coupling across spatial, feature, and temporal dimensions, facilitating information exchange among multiple regions. This provides theoretical support and feasibility verification for the multidimensional feature interaction and extraction techniques for spatial load.
- (2) The case study results indicate that the proposed model improves prediction accuracy at different time steps and demonstrates stronger stability under various adjacency matrix parameter settings. Compared to existing methods, it can more accurately predict the development trend of charging loads in different regions.
- (3) The visualization of the model's attention weights confirms the existence of spatial dependencies among user-level regions, enhancing the interpretability of the proposed model and facilitating further exploration of significant charging loads in the spatial domain.

This paper investigates electric vehicle user-level charging loads using a FastDTW-ASTGCN model with spatiotemporal data input. Future research will explore the use of multi-graph feature fusion to further extract charging characteristics for different types of electric vehicle users, aiming to improve the prediction accuracy.

Author Contributions: Conceptualization, Y.C. (Yang Chen) and Z.T.; methodology, Y.C. (Yibo Cui) and W.R.; validation, Y.L.; writing—original draft, Y.C. (Yang Chen); writing—review and editing, Z.T. and Y.C. (Yang Chen); supervision, Y.C. (Yibo Cui) and W.R. All authors have read and agreed to the published version of the manuscript.

Funding: This work was supported by the Technology Innovation Project of State Grid Hubei Electric Power Company (No. B3153221001D).

Data Availability Statement: The authors do not have permission to share data.

Conflicts of Interest: Z.T., Y.C. (Yibo Cui), W.R. and Y.L. were employed by State Grid Hubei Electric Power Research Institute. The remaining authors declare that the research was conducted in the absence of any commercial or financial relationships that could be construed as a potential conflict of interest.

Appendix A

Parameter settings for the adjacency matrices A_1 , A_2 , A_3 , A_4 , and A_* :

$$A_1 = \begin{bmatrix} 1 & 1 & 0 & 1 & 1 & 0 \\ 1 & 1 & 0 & 0 & 0 & 1 \\ 0 & 0 & 1 & 0 & 0 & 0 \\ 1 & 0 & 0 & 1 & 1 & 1 \\ 1 & 0 & 0 & 1 & 1 & 1 \\ 0 & 1 & 0 & 1 & 1 & 1 \\ 1 & 0 & 0 & 1 & 1 & 0 \\ 0 & 1 & 0 & 0 & 0 & 1 \\ 0 & 0 & 1 & 1 & 0 & 0 \\ 1 & 0 & 1 & 1 & 1 & 1 \\ 1 & 0 & 0 & 1 & 1 & 1 \\ 0 & 1 & 0 & 1 & 1 & 1 \end{bmatrix} \quad A_2 = \begin{bmatrix} 1 & 1 & 0 & 0 & 1 & 0 \\ 1 & 1 & 0 & 1 & 0 & 1 \\ 0 & 0 & 1 & 1 & 0 & 0 \\ 0 & 1 & 0 & 1 & 1 & 1 \\ 1 & 0 & 0 & 1 & 1 & 0 \\ 0 & 1 & 0 & 1 & 0 & 1 \end{bmatrix} \quad A_3 = \begin{bmatrix} 1 & 0 & 0 & 0 & 1 & 0 \\ 0 & 1 & 1 & 0 & 0 & 1 \\ 0 & 1 & 1 & 0 & 0 & 0 \\ 1 & 0 & 1 & 1 & 1 & 0 \\ 1 & 0 & 0 & 1 & 1 & 1 \\ 0 & 1 & 0 & 0 & 1 & 1 \end{bmatrix}$$

$$A_4 = \begin{bmatrix} 0 & 0 & 1 & 1 & 0 & 0 \\ 1 & 0 & 1 & 1 & 1 & 1 \\ 1 & 0 & 0 & 1 & 1 & 1 \\ 0 & 1 & 0 & 1 & 1 & 1 \end{bmatrix} \quad A_* = \begin{bmatrix} 0 & 0 & 1 & 0 & 0 & 0 \\ 0 & 0 & 0 & 1 & 1 & 0 \\ 1 & 0 & 0 & 1 & 1 & 0 \\ 0 & 1 & 0 & 0 & 0 & 1 \end{bmatrix}$$

References

1. Chen, L.; Zhang, Y.; Figueiredo, A. Overview of charging and discharging load forecasting for electric vehicles. *Autom. Electr. Power Syst.* **2019**, *43*, 177–191.
2. Fang, Y.; Hu, J.; Ma, W. Optimal dispatch strategy for electric vehicle aggregators based on Stackelberg game theory considering user intention. *Trans. China Electrotech. Soc.* **2024**, *39*, 5091–5103. [[CrossRef](#)]

3. Wang, H.; Yuan, J.; Chen, Z.; Ma, Y.; Dong, H.; Yuan, S.; Yang, J. Review and prospect of key techniques for vehicle-station-network integrated operation in smart city. *Trans. China Electrotech. Soc.* **2022**, *37*, 112–132.
4. Han, F.; Wang, X.; Qiao, J.; Shi, M.; Pu, T. Review on artificial intelligence based load forecasting research for the new-type power system. *Proc. CSEE* **2023**, *43*, 8569–8591.
5. Zhang, M.; Sun, Q.; Yang, X. Electric vehicle charging load prediction considering multi-source information real-time interaction and user regret psychology. *Power Syst. Technol.* **2022**, *46*, 632–641.
6. Lin, W.X.; Wu, D.; Boulet, B. Spatial-temporal residential short-term load forecasting via graph neural networks. *IEEE Trans. Smart Grid* **2021**, *12*, 5373–5384. [CrossRef]
7. Li, D.; Sun, G.; Miao, S.; Zhang, K.; Tan, Y.; Zhang, Y.; He, S. A short-term power load forecasting method based on multidimensional temporal information fusion. *Proc. CSEE* **2023**, *43* (Suppl. S1), 94–106.
8. Long, X.; Yang, J.; Wu, F.; Zhan, X.; Lin, Y.; Xu, J. Prediction of electric vehicle charging load considering interaction between road network and power grid and user's psychology. *Autom. Electr. Power Syst.* **2020**, *44*, 86–93.
9. Yang, B.; Wang, L.; Liao, C. Research on power-charging demand of large-scale electric vehicles and its impacting factors. *Trans. China Electrotech. Soc.* **2013**, *28*, 22–27.
10. Zhang, J.; Yan, J.; Liu, Y.Q.; Zhang, H.; Lv, G. Daily electric vehicle charging load profiles considering demographics of vehicle users. *Appl. Energy* **2020**, *274*, 115063. [CrossRef]
11. Lu, J.X.; Zhang, Q.P.; Yang, Z.H.; Tu, M. A hybrid model based on convolutional neural network and long short-term memory for short-term load forecasting. In Proceedings of the 2019 IEEE Power & Energy Society General Meeting (PESGM), Atlanta, GA, USA, 4–8 August 2019; pp. 1–5.
12. Wang, Y.; Gu, Y.; Ding, Z.; Li, S.; Wan, Y.; Hu, X. Charging demand forecasting of electric vehicles based on empirical mode decomposition-fuzzy entropy and ensemble learning. *Autom. Electr. Power Syst.* **2020**, *44*, 114–121.
13. Xie, X.; Zhou, J.; Zhang, Y.; Wang, J.; Su, J. WBiLSTM based ultra-short-term generation power prediction method of renewable energy. *Autom. Electr. Power Syst.* **2021**, *45*, 175–184.
14. Sun, W.; Zhu, S.; Yang, J.; Zhu, M.; Li, Q. Topology identification of microgrid based on graph convolutional network. *Autom. Electr. Power Syst.* **2022**, *46*, 71–81.
15. Zhu, N.; Wang, Y.; Yuan, K.; Yan, J.; Li, Y.; Zhang, K. GGNet: A novel graph structure for power forecasting in renewable power plants considering temporal lead-lag correlations. *Appl. Energy* **2024**, *364*, 123194. [CrossRef]
16. Hu, B.; Zhang, P.; Huang, E.; Liu, J.; Xu, J.; Xing, Z. Graph WaveNet based charging load forecasting of electric vehicles. *Autom. Electr. Power Syst.* **2022**, *46*, 207–213.
17. Luo, R.; Zhang, Y.; Zhou, Y.; Chen, H.; Yang, L.; Yang, J.; Su, R. Deep learning approach for long-term prediction of electric vehicle (EV) charging station availability. In Proceedings of the 2021 IEEE International Intelligent Transportation Systems Conference (ITSC), Indianapolis, IN, USA, 19–22 September 2021; pp. 3334–3339.
18. Zhuang, Y.R.; Cheng, L.; Qi, N.; Wang, X.Y.; Chen, Y. Real-time hosting capacity assessment for electric vehicles: A sequential forecast-then-optimize method. *Appl. Energy* **2025**, *380*, 125034. [CrossRef]
19. Mekkaoui, D.E.; Midoun, M.A.; Smaili, A.; Feng, B.W.; Talhaoui, M.Z.; Shen, Y.M. Probabilistic Dual-Adaptive Spatio-Temporal Graph Convolutional Networks for forecasting energy consumption dynamics of electric vehicle charging stations. *Comput. Electr. Eng.* **2025**, *122*, 109976. [CrossRef]
20. Xiao, B.; Li, P. Method for acquiring optimum spatial resolution of electric load. *Proc. CSEE* **2010**, *30*, 50–56.
21. Wuhan Metropolitan Main Function Zone Planning. Available online: https://zrzyhgh.wuhan.gov.cn/zwdt/gzdt/202110/t20211028_1821816.shtml (accessed on 16 December 2024).
22. Xiao, Y.; Zhao, Y.; Tu, Z.; Qian, B.; Chang, R. Verification method for the topology of low-voltage distribution network based on improved Pearson correlation coefficient. *Power Syst. Prot. Control.* **2019**, *47*, 37–43.
23. Yu, Q.; Huo, X.; He, J.; Li, L.; Zhang, J.; Feng, Y. Prediction of Power Outage Trends in China's Power Grid Based on Spearman's Correlation Coefficient and System Inertia. *Proc. CSEE* **2023**, *43*, 5372–5380.
24. Wang, D.; Shi, S.; Lu, J. Application of VMD-HD-KT Denoising Method in Pipeline Leakage Signal Denoising. *J. Jilin Univ. (Inf. Sci. Ed.)* **2023**, *41*, 202–206.
25. Feng, C.; Shao, L.; Wang, J.; Zhang, Y.; Wen, F. Short-term Load Forecasting of Distribution Transformer Supply Zones Based on Federated Model-Agnostic Meta Learning. *IEEE Trans. Power Syst.* **2025**, *40*, 31–45. [CrossRef]
26. Shuman, D.I.; Narang, S.K.; Frossard, P.; Ortega, A.; Vandergheynst, P. The emerging field of signal processing on graphs: Extending high-dimensional data analysis to networks and other irregular domains. *IEEE Signal Process. Mag.* **2013**, *30*, 83–98. [CrossRef]

Disclaimer/Publisher's Note: The statements, opinions and data contained in all publications are solely those of the individual author(s) and contributor(s) and not of MDPI and/or the editor(s). MDPI and/or the editor(s) disclaim responsibility for any injury to people or property resulting from any ideas, methods, instructions or products referred to in the content.